nature photonics

ARTICLES

PUBLISHED ONLINE: 17 MARCH 2013 | DOI: 10.1038/NPHOTON.2013.41

Quantum control of a spin qubit coupled to a photonic crystal cavity

Samuel G. Carter[1†], Timothy M. Sweeney[2†], Mijin Kim[3], Chul Soo Kim[1], Dmitry Solenov[2], Sophia E. Economou[1], Thomas L. Reinecke[1], Lily Yang[2], Allan S. Bracker[1] and Daniel Gammon[1*]

A key ingredient for a quantum network is an interface between stationary quantum bits and photons, which act as flying qubits for interactions and communication. Photonic crystal architectures are promising platforms for enhancing the coupling of light to solid-state qubits. Quantum dots can be integrated into a photonic crystal, with optical transitions coupling to photons and spin states forming a long-lived quantum memory. Many researchers have now succeeded in coupling these emitters to photonic crystal cavities, but there have been no demonstrations of a functional spin qubit and quantum gates in this environment. Here, we have developed a coupled cavity–quantum dot system in which the dot is controllably charged with a single electron. We perform the initialization, rotation and measurement of a single electron spin qubit using laser pulses, and find that the cavity can significantly improve these processes.

A solid-state optical cavity in a semiconductor photonic crystal membrane has many advantages for nanophotonics and cavity quantum electrodynamics (CQED)[1,2]. It can have a small volume and high quality factor Q (ref. 3), it can be combined with waveguides into extended and complex photonic architectures[3–5], and it can be integrated with semiconductor electronic devices[6–8]. In the last decade there has been rapid progress both in the development of photonic crystals themselves and in the study of solid-state emitters coupled to photonic crystal cavities[2–13]. Both quantum dots and nitrogen-vacancy centres can be incorporated into photonic crystal cavities and can have long-lived spin states[14,15]. This work has led to the vision of a quantum network[16], similar to that being developed for atomic systems[17], but in a scalable solid-state platform[18,19].

Proposals for quantum networks almost always involve quantum memories with three energy levels in a Λ configuration, that is, with two ground states and an optically excited state[16,18,19]. The two ground-state spin levels act as a long-lived quantum memory, and the optically excited state serves to connect the ground-state spin coherence to optical coherence. Yet, almost all experimental studies to date involving quantum dots in photonic crystal cavities and waveguides have used uncharged quantum dots, which essentially act as short-lived two-level systems. One way to obtain the Λ-type three-level system envisioned for a large-scale quantum network is to charge a quantum dot with a single electron. Recently, diodes have been incorporated into photonic crystal membranes[6–8] to serve this purpose, and one group has demonstrated controlled charging of a quantum dot in a cavity[20].

Although optical initialization, readout and quantum gates have already been demonstrated on spin qubits, doing so in the presence of a photonic crystal cavity presents both advantages and additional challenges. In particular, the photon density of states in a photonic crystal cavity is strongly modified from free space and is polarization-dependent. Here, we demonstrate complete quantum control of a quantum dot spin qubit coupled to a photonic crystal cavity. We show (1) controlled charging of a quantum dot in a cavity with a single electron using a diode incorporated into the photonic crystal; (2) the necessary Λ-type three-level system resulting from a magnetic field applied transverse to the sample; (3) spin measurement and initialization using resonant laser spectroscopy; and (4) single qubit gates with picosecond optical pulses. In fact, the polarization-dependent coupling of the cavity to the quantum dot has significant advantages for spin measurement and readout, and single qubit gates are demonstrated by detuning the pulses from the cavity resonance, thus avoiding polarization-dependent coupling.

Charged quantum dot coupled to a cavity

A photonic crystal membrane with a defect optical cavity (L3) was patterned and etched into an n-i-p (n-type, intrinsic, p-type) GaAs diode, into which InAs quantum dots had been grown in the intrinsic region, closer to the n-type layer (shown schematically in Fig. 1a). Charging of the quantum dots with a controlled number of electrons was performed by applying a forward bias across the diode. The charge state of a quantum dot was determined from its photoluminescence as a function of bias. A photoluminescence bias map of a quantum dot in a cavity (labelled QD-C1) (Fig. 1c) shows the neutral exciton (X^0), negatively charged exciton (X^-) and cavity lines. The X^- line, indicating a single electron in the quantum dot, is stable for a bias from 1.7 V to 1.95 V and is detuned from the cavity by 0.2–0.3 meV over this range. The cavity linewidth of ~0.3 meV corresponds to a quality factor Q of 4,000.

Resonant laser excitation of the quantum dot and the cavity mode was used to optically address and measure the spin states of the electron. The differential reflectivity[21,22] (ΔR) of a laser scanned across the X^-, cavity and X^0 resonances is presented in Fig. 1d,e; this was taken with two laser polarizations, parallel (V) and perpendicular (H) to the cavity polarization. The dominant feature at 1,301.93 meV for V polarization corresponds to the X^- line, which has a dispersive lineshape due to the proximity to the cavity mode and interference effects in the membrane. The cavity mode appears at ~1,302.1 meV as a broad (~0.3 meV) feature,

[1]Naval Research Laboratory, Washington, District of Columbia 20375, USA, [2]NRC Postdoctoral Associate Residing at the Naval Research Laboratory, Washington, District of Columbia 20375, USA, [3]Sotera Defense Solutions, Inc., Annapolis Junction, Maryland 20701, USA; [†]These authors contributed equally to this work. *e-mail: dan.gammon@nrl.navy.mil

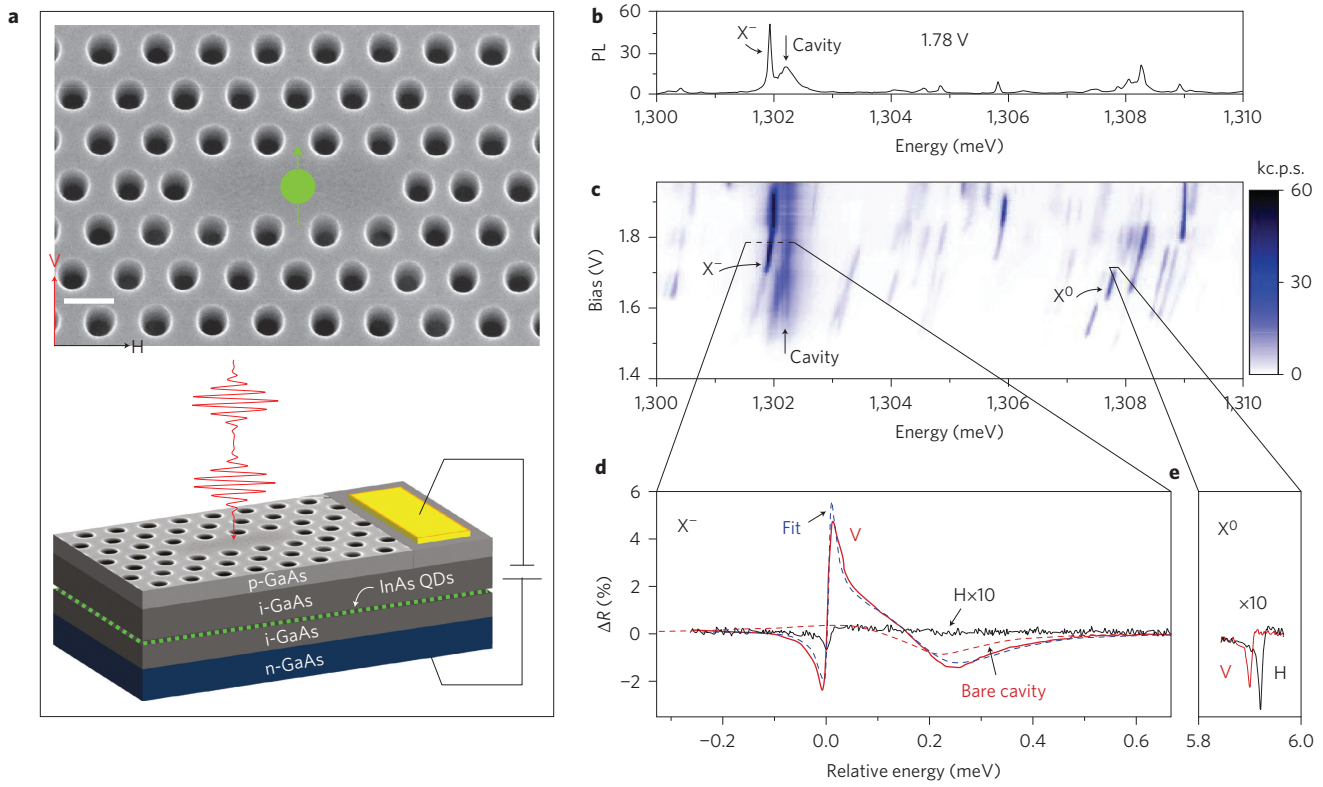

Figure 1 | Charged quantum dots in a cavity. a, Top: scanning electron micrograph of an L3 photonic crystal cavity with an illustration of an electron spin in the centre (actual quantum dot location is unknown). Scale bar, 200 nm. Bottom: illustration of the layers that form the n-i-p diode. **b**, Photoluminescence of the cavity–quantum dot system at a bias of 1.78 V and excitation at 1,391 meV. **c**, Photoluminescence bias map of the cavity–quantum dot system, measured in 1,000 counts per second (kc.p.s.). Horizontal lines correspond to the reflectivity scans below. **d**, Differential reflectivity near X^- at a bias of 1.785 V (solid lines), at which the quantum dot is charged with a single electron, and at 1.7 V (dashed red line), at which the quantum dot is uncharged. H and V correspond to the laser polarizations. **e**, Differential reflectivity of X^0 at 1.72 V. The magnetic field is zero, and the temperature is 7–8 K. The energy scale in **d** and **e** is relative to X^- at 1,301.93 meV.

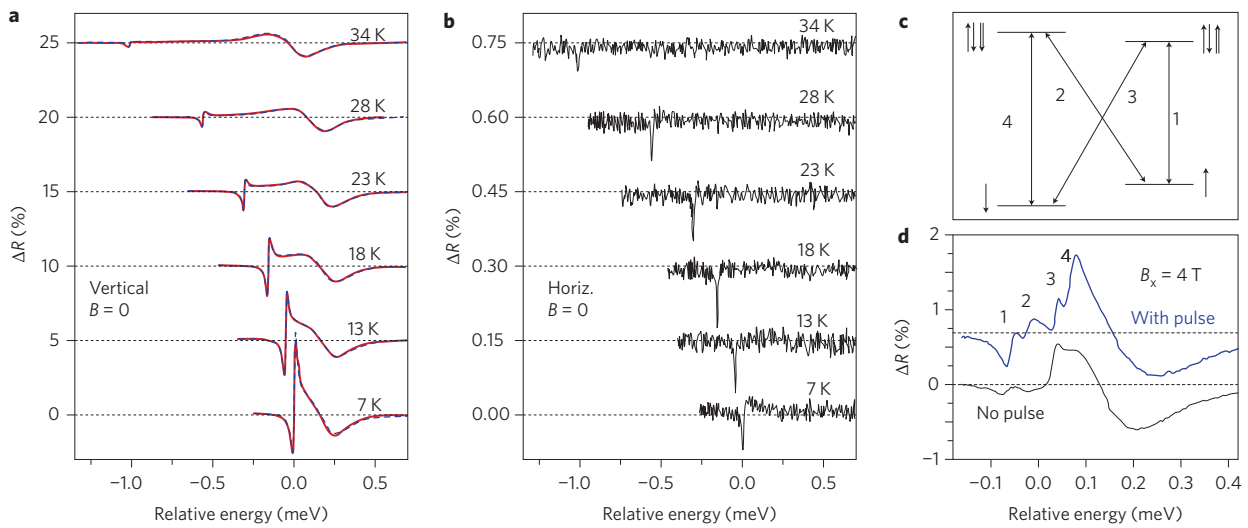

Figure 2 | Resonant laser spectroscopy. a,**b**, ΔR for V and H polarizations, respectively, for a series of temperatures, varying the detuning of X^- from the cavity. The dashed blue lines in **a** are fits to the reflectivity. The spectra are offset vertically at each temperature for clarity. **c**, Level diagram showing the electron spin states and X^- spin states in a Voigt magnetic field. Single (double) arrows represent electron (hole) spins. **d**, ΔR at $B_x = 4$ T for circular polarization with (upper curve) and without (lower curve) a short, resonant pulse that defeats optical pumping. The energy scales are relative to X^- at 7 K.

also with a highly dispersive lineshape, due primarily to the bias modulation in the differential technique. The coupling of X^- to the cavity is made evident by the order of magnitude increase in signal compared to X^0 and polarization anisotropy for the X^- signal. The optical response for V polarization is 70 times greater than for H. The ΔR for X^0 shows anisotropic exchange splitting[23], but the polarization anisotropy in the signal strength is essentially gone, because X^0 is detuned by 6 meV from the cavity resonance.

The linewidth of X^- is ~30 μeV, much greater than the 8 μeV linewidth of X^0 and ~30 times greater than the expected radiative limit for a quantum dot outside the cavity. We attribute this linewidth increase to the cavity–quantum dot interaction.

Figure 2a,b presents plots of ΔR for V and H polarizations for a series of temperatures, showing the behaviour as a function of cavity detuning. The X^- feature for V polarization decreases by a factor of 20 at 34 K (1 meV detuning), and the X^- line for H polarization decreases by a factor of only 2, reducing the polarization anisotropy. The X^- linewidth also decreases by as much as 30% with increasing temperature, consistent with a decrease in coupling to the cavity. The decrease in linewidth continues until 28 K, when the linewidth begins to increase, presumably due to phonon broadening. The ΔR for V polarization was fitted to a model that describes scattering of light from the coupled cavity–quantum dot system, including interference with background reflections (Supplementary Section SII.A). From these fits we obtained a cavity–dot coupling g_C of 25 μeV. This relatively small coupling strength is probably due to the modest spatial overlap between the quantum dot and cavity mode.

Spin initialization and measurement

To achieve spin measurement and initialization, a transverse magnetic field was applied to split the electron and X^- energy levels. This resulted in the four transitions shown in Fig. 2c, which can be considered two Λ-type three-level systems (the two systems differing in the X^- spin state). In Fig. 2d, the lower ΔR signal shows the cavity mode with only some small ripples near the expected X^- transitions. This result is an indication of optical pumping[24–26]. When a laser is resonant with one of the transitions, a small change in reflectivity occurs if the system is in the spin state being optically driven, thus measuring the spin state. However, recombination to the other spin state can occur, so the quantum dot system is quickly pumped out of the spin state being driven and into the other, eliminating absorption from the quantum dot. This effect is used to initialize the spin qubit. The four optical transitions are experimentally observed in Fig. 2d only when an optical pulse resonant with all four transitions (upper curve) is present to counter the effects of optical pumping. The presence of some residual signal from the quantum dot without the pulse is probably due to incomplete pumping and interference effects.

To better characterize optical initialization, it is useful to moderately detune the quantum dot from the cavity resonance, making the four transitions easier to resolve. Temperature tuning can accomplish this, but optical pumping is defeated at higher temperatures by faster spin relaxation. Instead, we examine a different quantum dot–cavity system (QD-C2) (Fig. 3), in which X^- is 1 meV above the cavity resonance at 7 K. In Fig. 3a, ΔR for V polarization is three times larger than for H, indicating the quantum dot is coupled to the cavity. At a magnetic field of 4 T (Fig. 3a, inset), the four transitions are observed with strong polarization dependence. We note that in our quantum dots the polarization axis is randomly oriented, presumably due to valence band mixing[25,27]. For this particular quantum dot, the axis is close to the cavity orientation, with the outer (inner) transitions predominantly coupling to V (H). For QD-C1 the axis is closer to 45°, so all four transitions couple well to the cavity.

To eliminate the dispersive lineshapes in ΔR that make it difficult to extract initialization fidelities, we measured the differential resonance fluorescence[28,29] (ΔRF, Supplementary Section SI.B) of QD-C2 by exciting with H polarization and detecting V, blocking out the reflected laser. Resonance fluorescence provides a nearly background-free alternative to ΔR as a way to measure the spin state. Instead of measuring a small change in reflectivity when the system is in the spin state being optically driven, photons are only scattered and detected when in that spin state. In Fig. 3b, on the edges of the charge stability region (1.87 V and 1.97 V) where

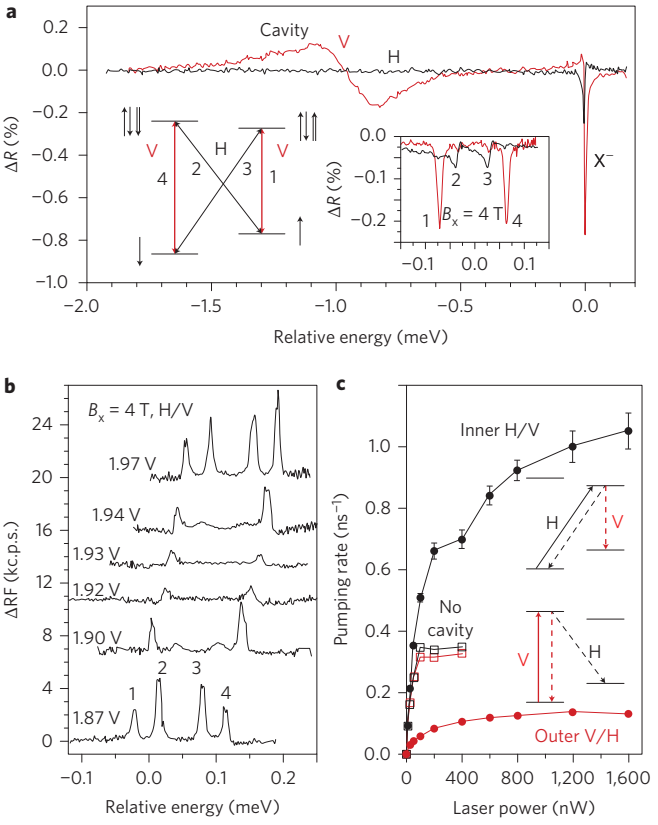

Figure 3 | Spin initialization and measurement in QD-C2. a, ΔR for H and V laser polarizations at zero magnetic field and a bias of 1.9 V. Inset: plot of ΔR of the X^- lines at $B_x = 4$ T and 1.87 V. The inset level diagram shows the electron spin states and X^- spin states in a Voigt magnetic field. Single (double) arrows represent electron (hole) spins. Thicker red lines indicate cavity-enhanced transitions. **b**, ΔRF for H polarized laser, V polarized detection for a series of biases (400 mV modulation) at $B_x = 4$ T and laser power of 25 nW. Spectra are offset vertically according to bias. **c**, Spin pumping rates versus laser power for inner/outer transitions for QD-C2 at 1.93 V and a quantum dot outside the cavity. The laser/detection polarization is H/V (V/H) for inner (outer) transitions. Error bars represent the standard error of the nonlinear least-squares fit to an exponential and are shown when larger than the data points. Inset level diagrams illustrate the effect of cavity enhancement on pumping rates. Solid (dashed) lines indicate the excitation laser (spontaneous emission).

rapid co-tunnelling occurs[25], all four transitions appear. Nominally, the outer transitions should not appear for H excitation, but the polarization selection rules are not perfectly aligned with H/V, and the cavity enhances emission for these transitions. As the bias moves towards the centre of the charge stability region, the inner transitions disappear due to optical pumping, giving an initialization fidelity of at least 95%. The outer transitions never entirely disappear because they are driven much more weakly with H polarization, and because the pumping rate is significantly slower for these transitions, as we will now show.

An important feature of the cavity is that the pumping rate is strongly modified, but in an asymmetric way. This is illustrated in the insets to Fig. 3c. When driving an outer (V) transition (lower diagram), which is more strongly coupled to the cavity, emission is likely to return the system to its initial spin state, thus giving a slow pumping rate. When driving an inner (H) transition (upper diagram), emission is more likely to change the spin state, thus giving a fast pumping rate. We determine these rates by temporally resolving the bleaching of RF due to optical pumping after a short

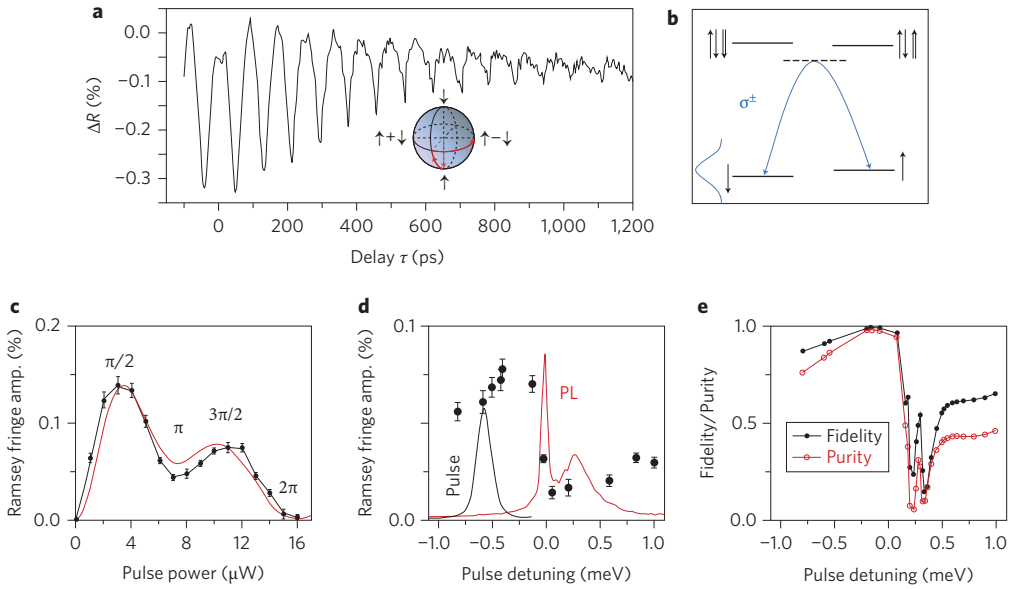

Figure 4 | Coherent spin rotation. a, Ramsey interference fringes at $B_x = 2$ T for a pulse detuning of −0.34 meV, with the initialization/measurement laser near transition 2. Inset: Bloch sphere with rotation of the Bloch vector from the first pulse and precession between pulses. **b**, Level diagram showing the coherent Raman process that couples the two electron spin states through an X^- state. The dashed line represents a virtual state. **c**, Fitted amplitude of the Ramsey interference fringes as a function of pulse power, for a detuning of −0.56 meV. The red curve is a model calculation. **d**, Maximum Ramsey fringe amplitude (solid circles) as a function of pulse detuning. The photoluminescence (PL) spectrum (at $B = 0$) and a sample pulse spectrum are displayed for comparison. Error bars in **c** and **d** represent the standard error of the nonlinear least-squares fit to a decaying cosine. **e**, Theoretical model of the fidelity of the spin rotation and purity of the resulting state as a function of pulse detuning.

pulse depolarizes the spin. In Fig. 3c, the optical pumping rates are plotted as functions of laser power for the laser tuned to the inner and outer transitions, with pumping rates for a quantum dot outside the cavity plotted for comparison. The pumping rate at saturation is an order of magnitude higher for the inner transitions than for the outer, even with moderate detuning. Thus, driving the transitions that are not coupled to the cavity permits fast initialization, and driving the transitions coupled to the cavity is better for spin measurement. For enhanced measurement it is especially advantageous to have well-aligned polarization axes and large Purcell enhancement. Optimizing these would give a cycling transition that could permit single-shot readout.

Ultrafast single qubit gates

A functional spin qubit also requires single qubit gates (that is, spin rotations). This is accomplished with short, circularly polarized pulses that couple the two spin states together through one of the two X^- spin states (Fig. 4b)[19,30–37]. A significant complication is that the cavity only couples to V polarization, and yet the rotation requires circular polarization. We find that spectrally detuning the pulse from the cavity alleviates this issue. The pulse then primarily interacts with the quantum dot directly instead of through the cavity mode.

To demonstrate these coherent rotations, we measured the spin population after two rotation pulses (∼13 ps length, ∼150 μeV bandwidth) delayed with respect to each other by a variable time τ (ref. 32). The resulting Ramsey interference fringes for QD-C1 are displayed in Fig. 4a. The first pulse rotates the Bloch vector near the equator, where it precesses (Fig. 4a, inset) for time τ at the Larmor precession frequency. The second pulse rotates the spin up or down depending on the phase, giving rise to oscillations in the spin population. The decay time of the oscillations (∼400 ps) is due primarily to dephasing from the fluctuating nuclear polarization[38]. It should be possible to recover the spin coherence using spin echo techniques[39] or by optically suppressing nuclear spin fluctuations[40,41]. In Fig. 4c, the amplitude of the Ramsey fringes is plotted as a function of rotation pulse power and is indicative of damped Rabi oscillations of the electron spin. The peaks at 3 μW and 11 μW correspond to rotation pulses with areas of $\pi/2$ and $3\pi/2$, respectively. The troughs at 7 μW and 15 μW correspond to rotations of π and 2π. The non-zero amplitude of the Ramsey oscillations for two nominal π pulses is due to precession during the pulses, which limits rotation fidelity. Simulations of the Ramsey fringes (displayed in Fig. 4c) give a similar behaviour due to this effect.

To determine how the cavity affects the pulse rotation, the maximum Ramsey fringe amplitude (that is, for $\sim\pi/2$ rotation pulses) was measured as a function of detuning, as shown in Fig. 4d. The amplitude is highly asymmetric about the quantum dot transitions at 1,301.95 meV. For negative pulse detunings, where the pulses are far from the cavity mode, the Ramsey fringes are strong, and for positive detunings, where the pulses are nearly resonant with the cavity mode, the fringes are quite weak. We compare this result to a theoretical model in which the incident laser field is modified by the cavity mode (Supplementary Section SII.C). Figure 4e plots the theoretical fidelity of a single pulse $\pi/2$ spin rotation and the purity of the resulting spin state after the pulse within this model. The calculations show behaviour qualitatively similar to the experiment. The poor fidelity near the cavity resonance arises from real excitation of X^- through the cavity, whereupon recombination destroys the purity of the spin state. The increase in fidelity at a detuning of 0.3 meV is due to the cavity field driving the system up to X^- and then partially back down to the ground states, preventing recombination. Both measurement and theory show that the fidelity can be quite high with a large negative detuning, such that the pulse is spectrally far away from the cavity.

Discussion

We have demonstrated the first functional spin qubit coupled to an optical cavity in which optical initialization, control and readout of an electron spin is achieved. Having a long-lived solid-state spin qubit coupled to a cavity opens up many areas of research including

CQED with a spin degree of freedom, spin-controlled photonics, and quantum networks. This type of system may in fact be used as a node in a quantum network, with optical pulses controlling the emission of photons into nearby waveguides, transmitting quantum states to other nodes[19]. An important step in this direction will be to provide better control over the parameters of the system, including spectral and spatial overlap with the cavity mode, higher Q-factors, and the polarization axis of the quantum dot relative to the cavity mode. Based on the pumping rates measured here, it seems possible with improved Q-factors and coupling strengths to drastically decrease the initialization time to picosecond timescales, significantly improving qubit operation speed. Also, with the quantum dot polarization axis better aligned to the cavity polarization, the cavity-enhanced transitions should act as very bright cycling transitions that could be used for single-shot readout. Previously, the only demonstrated quantum dot spin system with both fast spin initialization and cycling transitions was the W-system obtained in coupled quantum dots[26,29].

We also anticipate the incorporation of multiple spin qubits within a node. This can be achieved using quantum dot molecules in a cavity, where a tunnelling interaction provides two qubit gates[35,36]. Even without tunnel coupling, multiple quantum dot spin qubits within a cavity can be entangled using pulse sequences that make use of a cavity-induced interaction[42]. These multiple qubits can be used for error correction and form the basis of a quantum repeater or quantum computer.

Methods

Sample structure. The samples were grown by molecular beam epitaxy on n-type GaAs substrates. A 500 nm sacrificial layer of n-$Al_{0.7}Ga_{0.3}As$ was grown on the substrate, followed by 50 nm n-GaAs, 40 nm intrinsic GaAs, 3 nm InAs quantum dots, 50 nm intrinsic GaAs and 30 nm p-GaAs. The quantum dots were distributed randomly in the growth plane with a density of several quantum dots per μm^2. A positive electron-beam resist (ZEP520A, Zeon Chemicals) was used to define two-dimensional photonic crystals using a Raith 150 electron-beam lithography system, followed by Cl_2-based inductively coupled plasma etching. A triangular lattice of holes (radii, 70 nm) with a lattice spacing of 242 nm were etched through the epilayer into the AlGaAs, with three missing holes at the centre forming an L3 cavity (Fig. 1a). The AlGaAs under each photonic crystal was etched away, leaving a 180-nm-thick photonic crystal membrane. Ohmic contact was made to the p-type layer on the surface and to the n-type substrate.

Measurement techniques. The sample was mounted on piezo-stages in a magneto-optical cryostat, with the magnetic field oriented parallel to the long dimension of the cavity. A 0.68 NA aspheric lens focused lasers onto the sample and collected photoluminescence and reflected laser light. For ΔR measurements, the bias of the diode was modulated at 1–10 kHz with a square-wave peak-to-peak amplitude of ~200–400 mV, and the modulation of the reflected light was measured with lock-in detection. Small shifts in the cavity position with bias give rise to a ΔR signal from the cavity that was essentially the derivative with respect to bias, giving rise to dispersive lineshapes.

For Ramsey interference fringe measurements, the c.w. laser was used to initialize the system and read out the spin state. Pulses from the Ti:sapphire laser were split into two 13 ps pulses with circular polarization opposite to the c.w. laser, so that in detection the pulses were rejected using a polarizer. The c.w. laser was on between the pulses, which may have led to some decoherence. This effect appeared to be negligible compared to the effects from nuclear spins.

Received 9 July 2012; accepted 30 January 2013; published online 17 March 2013

References

1. Vahala, K. J. Optical microcavities. *Nature* **424,** 839–846 (2003).
2. Noda, S., Fujita, M. & Asano, T. Spontaneous-emission control by photonic crystals and nanocavities. *Nature Photon.* **1,** 449–458 (2007).
3. Notomi, M. Manipulating light with strongly modulated photonic crystals. *Rep. Prog. Phys.* **73,** 096501 (2010).
4. Englund, D., Faraon, A., Zhang, B. Y., Yamamoto, Y. & Vuckovic, J. Generation and transfer of single photons on a photonic crystal chip. *Opt. Express* **15,** 5550–5558 (2007).
5. Bose, R., Sridharan, D., Kim, H., Solomon, G. S. & Waks, E. Low-photon-number optical switching with a single quantum dot coupled to a photonic crystal cavity. *Phys. Rev. Lett.* **108,** 227402 (2012).
6. Francardi, M. *et al.* Enhanced spontaneous emission in a photonic-crystal light-emitting diode. *Appl. Phys. Lett.* **93,** 143102 (2008).
7. Laucht, A. *et al.* Electrical control of spontaneous emission and strong coupling for a single quantum dot. *New J. Phys.* **11,** 023034 (2009).
8. Englund, D. *et al.* An optical modulator based on a single strongly coupled quantum dot–cavity system in a p-i-n junction. *Opt. Express* **17,** 18651–18658 (2009).
9. Yoshie, T. *et al.* Vacuum Rabi splitting with a single quantum dot in a photonic crystal nanocavity. *Nature* **432,** 200–203 (2004).
10. Badolato, A. *et al.* Deterministic coupling of single quantum dots to single nanocavity modes. *Science* **308,** 1158–1161 (2005).
11. Hennessy, K. *et al.* Quantum nature of a strongly coupled single quantum dot–cavity system. *Nature* **445,** 896–899 (2007).
12. Wolters, J. *et al.* Enhancement of the zero phonon line emission from a single nitrogen vacancy center in a nanodiamond via coupling to a photonic crystal cavity. *Appl. Phys. Lett.* **97,** 141108 (2010).
13. Faraon, A., Santori, C., Huang, Z., Acosta, V. & Beausoleil, R. Coupling of nitrogen-vacancy centers to photonic crystal cavities in monocrystalline diamond. *Phys. Rev. Lett.* **109,** 033604 (2012).
14. Kroutvar, M. *et al.* Optically programmable electron spin memory using semiconductor quantum dots. *Nature* **432,** 81–84 (2004).
15. Balasubramanian, G. *et al.* Ultralong spin coherence time in isotopically engineered diamond. *Nature Mater.* **8,** 383–387 (2009).
16. Cirac, J. I., Zoller, P., Kimble, H. J. & Mabuchi, H. Quantum state transfer and entanglement distribution among distant nodes in a quantum network. *Phys. Rev. Lett.* **78,** 3221–3224 (1997).
17. Ritter, S. *et al.* An elementary quantum network of single atoms in optical cavities. *Nature* **484,** 195–201 (2012).
18. Imamoglu, A. *et al.* Quantum information processing using quantum dot spins and cavity QED. *Phys. Rev. Lett.* **83,** 4204–4207 (1999).
19. Liu, R. B., Yao, W. & Sham, L. J. Quantum computing by optical control of electron spins. *Adv. Phys.* **59,** 703–802 (2010).
20. Pinotsi, D., Fallahi, P., Miguel-Sanchez, J. & Imamoglu, A. Resonant spectroscopy on charge tunable quantum dots in photonic crystal structures. *IEEE J. Quant. Electron.* **47,** 1371–1374 (2011).
21. Alen, B., Bickel, F., Karrai, K., Warburton, R. & Petroff, P. Stark-shift modulation absorption spectroscopy of single quantum dots. *Appl. Phys. Lett.* **83,** 2235–2237 (2003).
22. Alen, B. *et al.* Absorptive and dispersive optical responses of excitons in a single quantum dot. *Appl. Phys. Lett.* **89,** 123124 (2006).
23. Gammon, D., Snow, E. S., Shanabrook, B. V., Katzer, D. S. & Park, D. Fine structure splitting in the optical spectra of single GaAs quantum dots. *Phys. Rev. Lett.* **76,** 3005–3008 (1996).
24. Atature, M. *et al.* Quantum-dot spin-state preparation with near-unity fidelity. *Science* **312,** 551–553 (2006).
25. Xu, X. *et al.* Fast spin state initialization in a singly charged InAs–GaAs quantum dot by optical cooling. *Phys. Rev. Lett.* **99,** 097401 (2007).
26. Kim, D. *et al.* Optical spin initialization and nondestructive measurement in a quantum dot molecule. *Phys. Rev. Lett.* **101,** 236804 (2008).
27. Koudinov, A., Akimov, I., Kusrayev, Y. & Henneberger, F. Optical and magnetic anisotropies of the hole states in Stranski–Krastanov quantum dots. *Phys. Rev. B* **70,** 241305(R) (2004).
28. Muller, A. *et al.* Resonance fluorescence from a coherently driven semiconductor quantum dot in a cavity. *Phys. Rev. Lett.* **99,** 187402 (2007).
29. Vamivakas, A. *et al.* Observation of spin-dependent quantum jumps via quantum dot resonance fluorescence. *Nature* **467,** 297–300 (2010).
30. Economou, S. E. & Reinecke, T. L. Theory of fast optical spin rotation in a quantum dot based on geometric phases and trapped states. *Phys. Rev. Lett.* **99,** 217401 (2007).
31. Berezovsky, J., Mikkelsen, M. H., Stoltz, N. G., Coldren, L. A. & Awschalom, D. D. Picosecond coherent optical manipulation of a single electron spin in a quantum dot. *Science* **320,** 349–352 (2008).
32. Press, D., Ladd, T. D., Zhang, B. Y. & Yamamoto, Y. Complete quantum control of a single quantum dot spin using ultrafast optical pulses. *Nature* **456,** 218–221 (2008).
33. Greilich, A. *et al.* Ultrafast optical rotations of electron spins in quantum dots. *Nature Phys.* **5,** 262–266 (2009).
34. Kim, E. D. *et al.* Fast spin rotations by optically controlled geometric phases in a charge-tunable InAs quantum dot. *Phys. Rev. Lett.* **104,** 167401 (2010).
35. Kim, D., Carter, S. G., Greilich, A., Bracker, A. S. & Gammon, D. Ultrafast optical control of entanglement between two quantum-dot spins. *Nature Phys.* **7,** 223–229 (2011).
36. Greilich, A., Carter, S. G., Kim, D., Bracker, A. S. & Gammon, D. Optical control of one and two hole spins in interacting quantum dots. *Nature Photon.* **5,** 703–709 (2011).
37. Godden, T. M. *et al.* Coherent optical control of the spin of a single hole in an InAs/GaAs quantum dot. *Phys. Rev. Lett.* **108,** 017402 (2012).

38. Ladd, T. D. *et al.* Pulsed nuclear pumping and spin diffusion in a single charged quantum dot. *Phys. Rev. Lett.* **105,** 107401 (2010).
39. Press, D. *et al.* Ultrafast optical spin echo in a single quantum dot. *Nature Photon.* **4,** 367–370 (2010).
40. Greilich, A. *et al.* Nuclei-induced frequency focusing of electron spin coherence. *Science* **317,** 1896–1899 (2007).
41. Sun, B. *et al.* Persistent narrowing of nuclear-spin fluctuations in InAs quantum dots using laser excitation. *Phys. Rev. Lett.* **108,** 187401 (2012).
42. Solenov, D., Economou, S. E. & Reinecke, T. L. Fast two-qubit gates for quantum computing in semiconductor quantum dots using a photonic microcavity. *Phys. Rev. B* **87,** 035308 (2013).

Acknowledgements

This work was supported by a Multi-University Research Initiative (US Army Research Office; W911NF0910406), the NSA/LPS, and the US Office of Naval Research. The authors thank A. Greilich for contributions during the preliminary stage of this research.

Author contributions

All authors were involved in preparing the manuscript. S.G.C., T.M.S., A.S.B. and D.G. conceived and designed the experiments and samples. A.S.B. grew the quantum dot samples. M.K., C.S.K. and A.S.B. processed photonic crystals and gates in the samples. T.M.S., S.G.C. and L.Y. optically characterized the cavities and quantum dots. S.G.C. performed the differential reflectivity and laser control experiments. D.S., S.E.E., T.L.R. and T.M.S. provided theoretical insight and calculations.

Additional information

Supplementary information is available in the online version of the paper. Reprints and permissions information is available online at www.nature.com/reprints. Correspondence and requests for materials should be addressed to D.G.

Competing financial interests

The authors declare no competing financial interests.